Hollow carbon spheres for diclofenac and venlafaxine adsorption

Ana Luísa S. Vieira, Rui S. Ribeiro*, Ana R. Lado Ribeiro, Adrián M.T. Silva

Laboratory of Separation and Reaction Engineering - Laboratory of Catalysis and Materials (LSRE-LCM), Faculdade de Engenharia, Universidade do Porto, Rua Dr. Roberto Frias, 4200-465 Porto, Portugal.

*Corresponding author. E-mail address: rsribeiro@fe.up.pt

This article has been accepted for publication and undergone full peer review.
Please cite this article as DOI: 10.1016/j.jece.2022.107348.

Abstract

Silica@polymer spheres with a core@shell structure were synthesized and thermally annealed at 800 ºC to obtain silica@carbon spheres (SiO_2@CSs). The silica core was then removed by etching with sodium hydroxide and hollow carbon spheres (CSs) were thus obtained. The particle size of both SiO_2@CSs and CSs increased with the ethanol/water (E/W) volumetric ratio (2, 4.5, and 7) employed in the first synthesis step (*i.e.*, during the application of the Stöber's method to obtain silica particles). Moreover, the average diameter of the materials prepared with E/W ratio of 2 was affected by the etching of the SiO_2 core (from 168 to 109 nm), in contrast with those synthesized at higher E/W ratios of 4.5 and 7 (251 to 245 and 270 to 284 nm, respectively). The specific surface area (S_{BET}) of the CSs ranged from 271 to 602 m^2 g^{-1}, which are more porous than SiO_2@CSs (S_{BET} in the range 115 to 144 m^2 g^{-1}). Adsorption kinetic and equilibrium studies were then carried out with diclofenac and venlafaxine as model organic micropollutants (OMPs). Despite the silica removal was not effective for all the CSs prepared (TGA residue ranging from 3 to 46 wt.%), the kinetic studies confirmed the positive effect of having a hollow core (*i.e.*, removing the silica core). Equilibrium studies demonstrated that CSs prepared with an E/W volumetric ratio of 7 were the best performing material when considering both OMPs. Thus, these CSs are an interesting option for water or wastewater treatment.

Keywords

Silica-carbon spheres; Hollow spheres; Diclofenac; Venlafaxine; Adsorption.

Abbreviations

BET, Brunauer–Emmett–Teller; BSE, backscattered electron; CEC, contaminant of emerging concern; CSs, carbon spheres; DCF, diclofenac; EDS, energy-dispersive X-ray spectroscopy;

EU, European Union; E/W, ethanol/water; F, formaldehyde; HPLC, high-performance liquid chromatography; HS, hydroxymethyl-substituted; NMs, nanomaterials; OMP, organic micropollutant; PS, priority substance; R, resorcinol; RF, resorcinol-formaldehyde; SE, secondary electron; SEM, scanning electron microscopy; SEM-EDS, Scanning electron microscopy coupled to energy-dispersive X-ray spectroscopy; TEOS, tetraethyl orthosilicate; TGA, thermogravimetric analysis; VFX, venlafaxine; WFD, Water Framework Directive; WWTP, wastewater treatment plant.

1. Introduction

Over the last few decades, the occurrence of pollutants in the aquatic environment has raised increasing concern due to the possible impact on wildlife and human health [1,2]. Organic micropollutants (OMPs) are usually present in aquatic compartments at trace concentrations [2]. Among these OMPs, we can find food additives, industrial and household chemicals, pharmaceuticals and personal care products [2,3].

In order to protect water, the European Parliament and Council introduced the Directive 2000/60/EC in 2000, also known as the European Union (EU) Water Framework Directive (WFD) [4], which was amended together with Directive 2008/105/EC. In 2013, Directives 2000/60/EC and 2008/105/EC were revised, and the most recent Directive 2013/39/EU included a list of 45 priority substances (PSs), highlighting the demand for innovative water treatment solutions and the importance of monitoring contaminants of emerging concern (CECs) for which legislation does not exist yet. In this regard, the Decision 2015/495/EU established a watch list of 10 CECs that was updated by Decision 2018/840/EU and, more recently, by Decision 2020/1161/EU, specifying the CECs that should be monitored and considered for inclusion in the future regulatory revisions [5].

Some pharmaceuticals have been included in these dynamic watch lists due to the growing environmental concern related to their recalcitrance upon degradation in conventional wastewater treatment plants (WWTPs), and thus representing a continuous input into the environment [6]. For instance, the rate of elimination of diclofenac (DCF) and venlafaxine (VFX) in conventional sewage treatment plants has been reported as being low (up to 40%) [7,8]. These drugs have a low hydrophobicity, as suggested by the octanol–water partitioning coefficients (log K_{ow}), and a relatively low Henry's law constant (Table S1). Thus, these compounds are less likely to volatilize into the atmosphere, which means that they tend to

persist in water [9]. It is noteworthy that due to the polar nature of most pharmaceuticals, they are not significantly adsorbed in the subsoil and may leach into the groundwater aquifers [10]. Therefore, these polar target compounds have a likely affinity to the water phase, with VFX having a higher solubility in water than DCF. Consequently, it becomes extremely difficult to remove these compounds by the conventional treatments applied at WWTPs.

Considering the water contamination concern, adsorption is considered one of the most adequate and applicable techniques for pollutant removal due to its simplicity and easy operation [11]. Carbon nanomaterials (NMs) have been used as sorbents because they possess a high surface area-to-volume ratio that usually guarantees much greater adsorption capacity, as well as the possibility to easily modify their surface chemistry to improve the selectivity towards the target adsorbates [12]. In fact, NMs can strongly adsorb many substances including trace metals and polar organic compounds [11,12].

Hollow carbon spheres (CSs) have gained increased interest for adsorption applications, especially because of their potential to store substances within their inner cavities. In order to confirm this hypothesis, different nanostructured CSs were synthetized in the present study, by adapting the procedure previously reported by Fuertes *et al.* [13]. These CSs were employed in adsorption studies, by selecting two model OMPs: the non-steroidal anti-inflammatory drug DCF and the serotonin-norepinephrine reuptake inhibitor VFX, due to their large consumption worldwide and their high detection frequency in aquatic environments [14–16]. In addition, DCF was one of the CECs of a previous watch list [17] and VFX has recently been included in the watch list of CECs defined by Decision 2020/1161/EU [18]. To study the adsorption kinetic behavior of DCF or VFX onto the CSs, fractional power, pseudo-first order, pseudo-second order, and Elovich models were fitted to the experimental data, allowing to understand the performance of the carbon materials. The Langmuir, Freundlich and Sips models were then employed to obtain valuable information from the adsorption isotherms, such as the adsorption

mechanisms, the maximum adsorption capacity, and the adsorbent properties [19]. To the best of our knowledge, both the effect of the hollow core, and the influence of the particle size of the CSs on the adsorption of DCF and VFX were herein studied for the first time.

2. Experiments

2.1. Chemicals and instruments

Tetraethyl orthosilicate (TEOS; 99 wt.%), resorcinol (99 wt.%) and formaldehyde solution (37 wt.% in H_2O, containing 10-15% of methanol as stabilizer) were obtained from Sigma–Aldrich. Ammonia aqueous solution (28% v/v), sodium hydroxide and absolute ethanol (99.9 wt.%) were purchased from VWR. Diclofenac (sodium salt) and venlafaxine hydrochloride were purchased from Cayman and Supelco, respectively. Sodium chloride (99.5 wt.%) was purchased from JMGS. Acetonitrile (HPLC grade) and formic acid (99 wt.%) were purchased from VWR and used for high-performance liquid chromatography (HPLC). Distilled water was used for the synthesis of CSs, whereas ultrapure water supplied by a Milli-Q water system was used in all the other experiments.

2.2. Synthesis of CSs

As referred above, silica@resorcinol–formaldehyde (SiO_2@RF) spheres were prepared by adapting the procedure described in the work of Fuertes *et al* [13]. Accordingly, 5 mL of ammonia aqueous solution (NH_4OH) was added to a mixture containing absolute ethanol and distilled water (ethanol/water (E/W) volume ratios of 2, 4.5 and 7; considering a total volume of 160 mL), and then maintained at 30 ºC for 30 min under stirring (240 rpm). Subsequently, under vigorous stirring at 350 rpm, the following chemicals were added: (i) 5.6 mL of TEOS ($Si(OC_2H_5)_4$), which was stirred for 10 min; (ii) 0.8 g of resorcinol, which was stirred for 10 min; and finally, (iii) 1.12 mL of formaldehyde solution. The reaction mixture was then

maintained at 30 ºC for 24 h under stirring (240 rpm), and at 100 ºC for 24 h under static conditions. Afterwards, the solid product was collected by centrifugation, washed with distilled water, and dried overnight at 100 ºC. The resulting material (SiO_2@RF spheres) was placed in a tubular vertical reactor with a porous plate and thermally annealed under a nitrogen flow (N_2, 100 cm^3 min^{-1}), at 3 sequential temperature steps of 60 min each (120 ºC, 400 ºC, and 600 ºC), followed by a period of 240 min at 800 ºC, with a heating rate set at 2 ºC min^{-1}. The carbonized product (SiO_2@CS) was treated in a strong basic solution of sodium hydroxide (NaOH, 10 mol L^{-1}) for 20 h at room temperature and under vigorous stirring to dissolve the silica core. For etching of silica from the core of the CSs, a proportion of 50 mL of NaOH per gram of SiO_2@CSs weighed was used. The sample was washed with distilled water and collected by centrifugation, several times until the neutrality of the rinsing waters was reached, and then dried overnight at 100 ºC. The resulting materials were denoted as SiO_2@RF_X or CS_X, in which *X* represents the E/W volume ratio used in the respective synthesis.

2.3. Characterization techniques

The morphology of the CSs was studied by scanning electron microscopy (SEM), using a FEI Quanta 400 FEG ESEM/EDAX Genesis X4M apparatus coupled with energy-dispersive X-ray spectroscopy (EDS). SEM images were obtained in secondary electron (SE) and backscattered electron (BSE) detection modes, operating at 25 kV. The surface morphology was observed at different magnifications (from 100000 to 150000 times). ImageJ software was used to estimate the diameter of the CSs (at least 75 counts were performed for each sample). The elemental composition of the CSs was studied by EDS.

Thermogravimetric analysis (TGA) was performed in a Netzsch STA 490 PC/4/H Luxx thermal analyzer, in which the sample (3 to 10 mg) was heated from 50 to 900 ºC at a rate of 10 ºC min^{-1}, under an oxidative (air) gas flow.

The textural characterization of the samples was based on adsorption-desorption isotherms of N_2 obtained at -196 ºC, which were performed in a Quantachrome Instruments Nova 4200e Surface Area and Pore Size Analyzer apparatus equipped with a NovaWin^{TM} software. Before analysis, the samples (~0.1 g) were outgassed at a heating rate of 2 ºC min^{-1}, starting from 50 ºC until reaching 130 ºC, and then left under vacuum for 6 h. The specific surface area (S_{BET}) of the materials were calculated by the Brunauer–Emmett–Teller (BET) method using adsorption isotherms for relative pressures (P/P_0) between 0.05 and 0.30. The non-microporous surface area (S_{Meso}) and the volume of micropores (V_{Micro}) were calculated by the *t*-method using the standard isotherms proposed by Thommes *et al.* [20]. The total pore volume (V_{Total}) was determined from the amount adsorbed at a relative pressure close to unity.

The pH at the point of zero charge (pH_{PZC}) of the materials was determined by pH drift tests, by adapting the procedure previously reported by Ribeiro *et al.* [21]. The samples (0.025 g) were then dispersed in these solutions, and the final pH was measured after 64 h of continuous stirring at room temperature (23 ± 1 ºC).

2.4. Kinetic and equilibrium adsorption experiments

Both adsorption kinetic and equilibrium studies were carried out at room temperature (23 ± 1 ºC), using a magnetic stirrer, and without pH conditioning, *i.e.*, considering the inherent pH of the DCF and VFX solutions (6.4 and 6.2, respectively).

In kinetic adsorption experiments, a mass of CSs (5 mg) corresponding to a concentration of adsorbent (C_{ads}) of 0.25 g L^{-1} was added to a DCF or VFX solution with an initial concentration (C_0) of 100 mg L^{-1} (20 mL), which was kept under stirring in a 30 mL amber flask. Samples were filtered before analysis through 0.2 μm polytetrafluoroethylene syringe filters at predetermined intervals.

Equilibrium adsorption isotherm experiments were carried out in a digital magnetic stirrer multiplace MultiMix D MM90E Ovan with a constant mass of adsorbent (2.5 mg) dispersed in a constant volume of a DCF or VFX solution (10 mL) at various initial concentrations (ranging from 1 to 100 mg L^{-1}), keeping the ratio adsorbent mass/solution volume constant. Each amber flask was loaded and then sealed for the predetermined period needed to reach the equilibrium. Upon equilibrium, the samples were filtered and analyzed.

2.5. Analytical procedures

The determination of DCF or VFX concentrations was performed using a Shimadzu HPLC apparatus equipped with fluorescence detector. The separation was performed in a Kinetex™ XB-C18 100 Å column (100 × 2.1 mm, i.d.; particle diameter of 1.7 μm) and the optimized mobile phase consisted of 0.1% (v/v) formic acid and acetonitrile, at a flow rate of 0.25 mL min^{-1} and under gradient mode. Column oven and autosampler temperatures were set respectively at 30 and 15 ºC, and the volume of injection was 10 μL. Those samples whose concentration was above the range of the calibration curves were diluted in ultrapure water and the dilution factor was considered for the estimation of the sample concentrations. The precision of the analytical procedure was considered, being repeatability less than 3% and reproducibility (intermediate precision) less than 1% for both OMPs.

3. Results and discussion

3.1. Mechanistic insights into the synthesis of CSs

The CSs were obtained by adapting the procedure reported by Fuertes *et al.*, namely the one-step synthesis of silica@resorcinol-formaldehyde (SiO_2@RF) spheres based on Stöber's conditions [13]. The Stöber's method is a pioneering approach for the synthesis of spherical and monodisperse silica nanoparticles of uniform size by hydrolysis and condensation of silicon alkoxides (*i.e.*, TEOS) in an E/W mixture, in the presence of ammonia as a catalyst [22]. Briefly, the synthesis of SiO_2@RF in a single step was possible since SiO_2 particles were formed first (higher reaction rate), and only then covered with resorcinol and formaldehyde (24 h at 30 ºC), which finally undergo a complete sol-gel polycondensation reaction at 100 ºC.

According to the literature, five parameters can influence the size (and size distribution) of spherical SiO_2 particles: (i) concentration of ammonia, (ii) concentration of TEOS, (iii) alcohol/water ratio, (iv) type of alcohol, and (v) temperature [22–26]. Fuertes *et al.* found that silica spheres are efficiently produced when employing E/W volumetric ratios equal or above 2 [13], whereas 7 was the highest E/W ratio used by Stöber *et al.* [22]. Moreover, Fuertes *et al.* reported that the E/W ratio was the parameter that most influences the size of the resulting SiO_2 particles [13]. Therefore, the effect of the E/W ratio selected in the synthesis on the particle size was studied in the present work, by varying the E/W ratio from 2 to 7. In this sense, the influence of particle size of hollow CSs on the adsorption of DCF and VFX was studied for the first time.

Once (i) SiO_2 spheres are obtained, the subsequent steps involved in the synthesis of hollow CSs are those depicted in Fig. 1, namely (ii) polymerization of resorcinol – R – with formaldehyde – F, (iii) carbonization, and (iv) etching of the SiO_2 core.

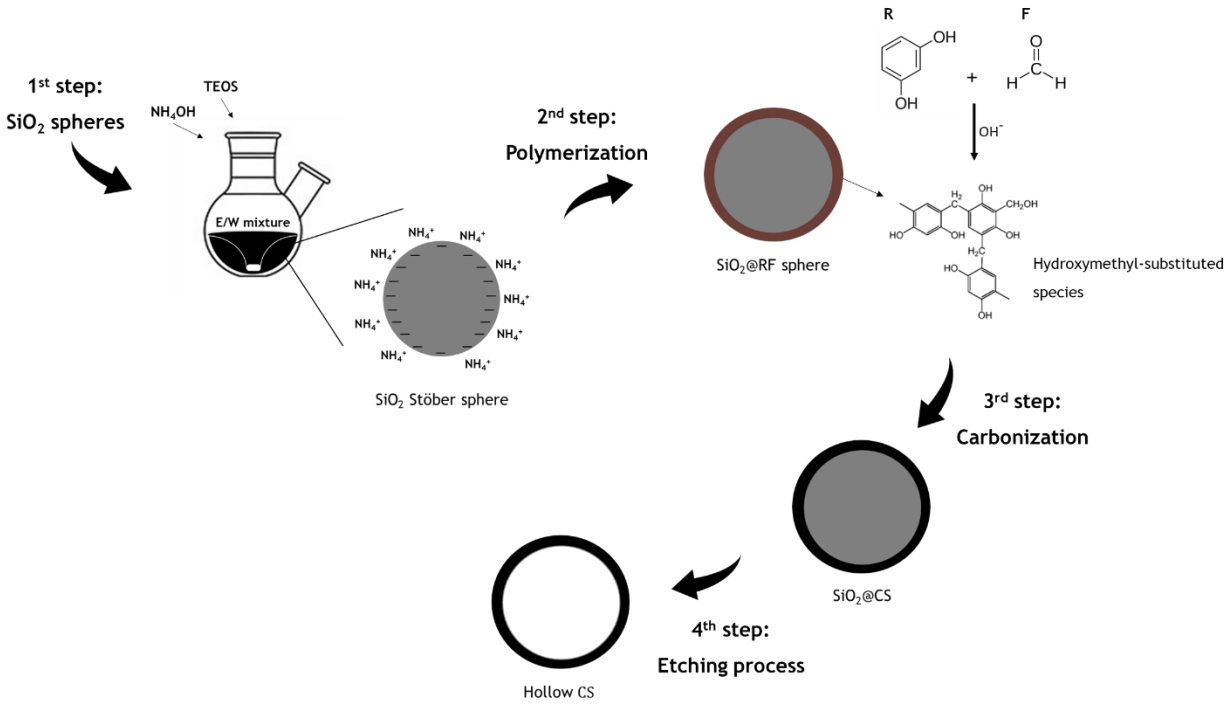

Fig. 1. Schematic representation of the synthesis of hollow CSs.

The fast formation of SiO_2 spheres occurs during the first stage of the synthesis procedure, by adding TEOS to an aqueous solution containing ethanol and ammonia (NH_4OH). A turbid white suspension started being formed about 10 min after TEOS was added (as can be seen in Fig. S1), suggesting the formation of a stable colloidal suspension of SiO_2 (*i.e.*, particle aggregation and/or sedimentation is negligible). This is due to the addition of ammonia, which is known to accelerate the polymerization of resorcinol with formaldehyde, but also to provide positive charges that adhere to the outer surface of the SiO_2 spheres, thus preventing aggregation between these spheres [25,27]. The NH_4^+ ions cover the surface of the silica particles, which are negatively charged. Moreover, ammonia influence the morphology of the resulting particles, leading to materials with spherical shape [22]. The second step (polymerization) was then initiated when both resorcinol and formaldehyde were added to the SiO_2 suspension. Resorcinol reacts with formaldehyde to form numerous hydroxymethyl-substituted (HS) species. This

reaction (catalyzed by HO^- ions) is much slower than the Stöber reaction and requires higher temperature to be completed (up to 100 ºC). Once formed, the HS species will gradually diffuse to the surface of the SiO_2 particles due to electrostatic interactions with the NH_4^+ ions attached to its surface, resulting in the formation of a first RF polymeric layer around the SiO_2 spheres. SiO_2@RF spheres with a core@shell structure were obtained as the polymerization reaction proceeded for 24 h at 30 ºC, and then 24 h at 100 ºC. Accordingly, a remarkable change in the solution color was observed during the polymerization step. The turbid white suspension of SiO_2 gradually became dark reddish-brown as SiO_2@RF spheres were formed (Fig. S1).

The third step of the synthesis of the CSs took place upon thermal annealing of the SiO_2@RF spheres at 800 ºC under N_2 atmosphere, through which the RF polymeric layer was carbonized while the SiO_2 core was unaffected. In the fourth and last step, the SiO_2 core of the carbonized product (SiO_2@CS) was removed by an etching process in a strong basic NaOH solution.

3.2. Characterization of CSs

SEM analysis was used to study the morphology, particle size and size distribution, as well as aggregation/dispersion of the synthesized materials. As observed in the SEM images given in Fig. 2, all the materials exhibited a spherical morphology, and the particles were well dispersed. It is also visible that the final hollow core, within the CSs, had a regular and smooth surface (Fig. 2d and f), except for CS_2 (Fig. 2b), in which a partial rupture of the spherical carbon shell apparently occurred during the etching process (*i.e.*, when testing the lower E/W volumetric ratio).

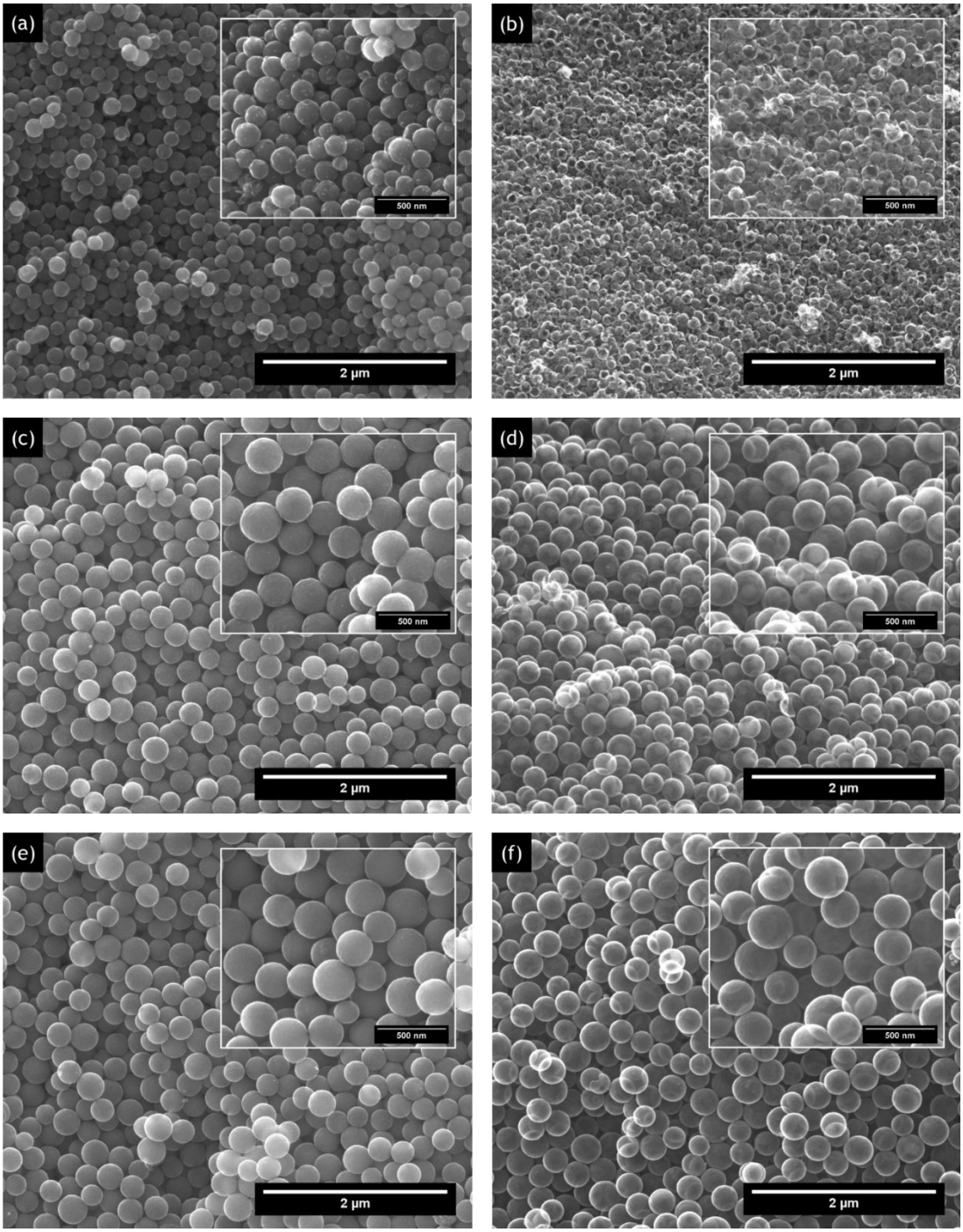

Fig. 2. SEM micrographs of: (a) $SiO_2@CS_2$, (b) CS_2, (c) $SiO_2@CS_{4.5}$, (d) $CS_{4.5}$, (e) $SiO_2@CS_7$, and (f) CS_7. Images obtained in SE mode.

As expected, the average diameter ($d_{average}$) of the CSs (Figs. 3 and S2) determined by SEM measurements, increased with the E/W ratio. Moreover, the $d_{average}$ before and after the SiO_2 dissolution step suggest that the CSs prepared with an E/W ratio of 2 had slightly shrunk during this process, *i.e.*, there was a decrease of the $d_{average}$ of SiO_2@CS_2 upon etching with NaOH, corresponding to around 54% of its initial size. In turn, the $d_{average}$ of the materials prepared with E/W ratios of 4.5 and 7 was negligibly affected by the etching of the SiO_2 core (Fig. 3), suggesting that the CSs are less resistant to the etching process only at the lower E/W ratio.

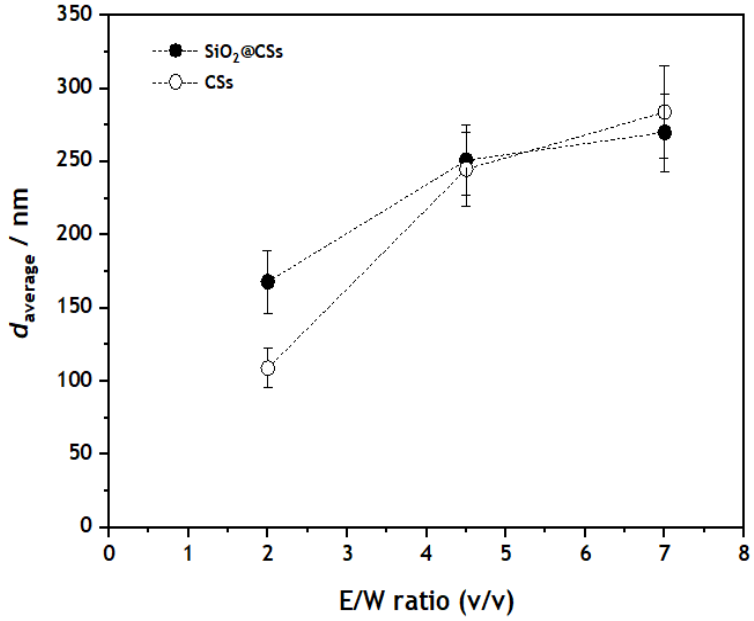

Fig. 3. Particle diameter of SiO_2@CSs and CSs as a function of the E/W ratio.

After the SiO_2 dissolution step, some transparencies were observed in the SEM micrographs (Fig. 2), *i.e.*, some CSs in the background can be observed through the outline of the carbon shell of CSs in the foreground. This feature is particularly clear for $CS_{4.5}$ and CS_7 (insets of Fig. 2d and f, respectively), suggesting that the dense SiO_2 cores were effectively removed upon dissolution with NaOH. Additional SEM micrographs were obtained in BSE mode (Fig. 4) and

under this detection mode, denser chemical elements were recorded as brighter regions in some micrographs, thus allowing to distinguish carbon from silica. Accordingly, large bright spheres are observed in the SEM micrographs of $SiO_2@CS_2$, $SiO_2@CS_{4.5}$ and $SiO_2@CS_7$ (Fig. 4a, c, and e, respectively), which correspond to the SiO_2 cores. On the contrary, almost no bright zones were found in the SEM micrographs of CS_2 and CS_7 (Fig. 4b and f, respectively), confirming the effectiveness of the silica etching process (in the case of CS_2 most probably due to the partial rupture of the spherical carbon shell). In the particular case of $CS_{4.5}$ (Fig. 4d), it is interesting to observe some small bright spheres inside the carbon shell, suggesting that the etching process of silica was not so effective in this case. In fact, EDS spectra (Fig. S3) showed that the predominant element in $SiO_2@CS_2$, $SiO_2@CS_{4.5}$ and $SiO_2@CS_7$ was silicon, whereas carbon was predominant in CS_2, $CS_{4.5}$ and CS_7. Nevertheless, some silicon was still present in $CS_{4.5}$ and CS_7, which agrees with the SEM observations. In addition, this elemental mapping analysis only shows trace amounts of the element sodium ($CS_{4.5}$ and CS_7), indicating that the washing step after the etching process was successful as well.

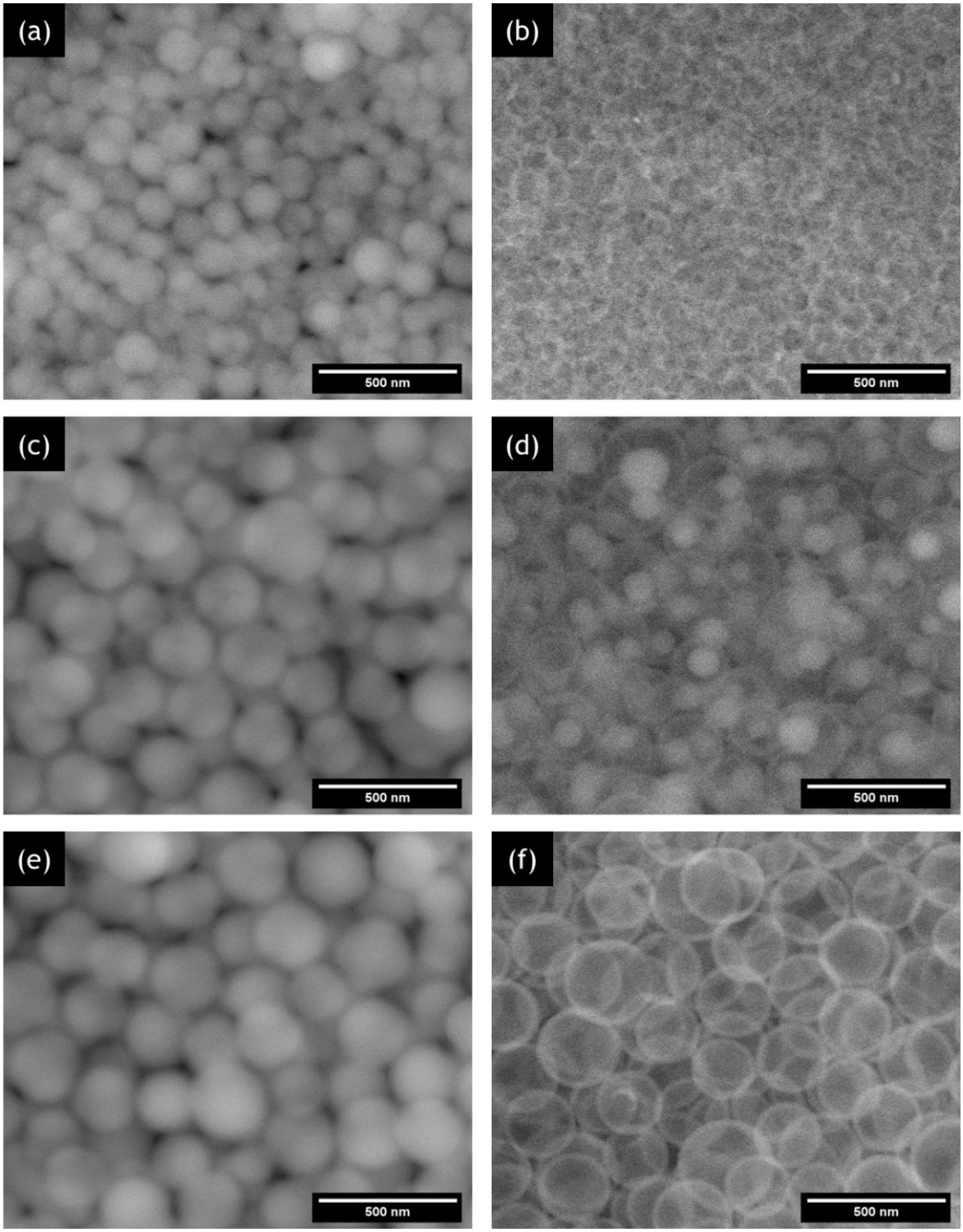

Fig. 4. SEM micrographs of: (a) $SiO_2@CS_2$, (b) CS_2, (c) $SiO_2@CS_{4.5}$, (d) $CS_{4.5}$, (e) $SiO_2@CS_7$, and (f) CS_7. Images obtained in BSE mode.

The results obtained by TGA under oxidative atmosphere (Table 1 and Fig. S4) agree with those obtained by SEM-EDS. All the SiO_2@CSs have a high ash content (TGA residue ranging from 76 to 81 wt.%), which can be ascribed to the SiO_2 core. On the contrary, CS_2 revealed a negligible ash content (3 wt.%), confirming that the treatment with NaOH successfully removed the SiO_2 core from this material. CS_7 has an ash content of 24 wt.%, whereas $CS_{4.5}$ presents a higher amount (46 wt.%). These results allow to conclude that the etching process was more effective in the case of CS_2, followed by CS_7; and not as effective in the case of $CS_{4.5}$.

Table 1. TGA residues and carbon content of the CSs, as determined by TGA under air atmosphere.

Sample	TGA residue / wt.%	Carbon content [a] / wt.%
SiO_2@CS_2	81	19
CS_2	3	97
SiO_2@$CS_{4.5}$	76	24
$CS_{4.5}$	46	54
SiO_2@CS_7	78	22
CS_7	24	76

[a] Estimated as the mass fraction not corresponding to ashes (TGA residue).

Considering the N_2 adsorption–desorption isotherms (Fig S5), all the materials possess both micropores (as indicated by the adsorption of N_2 at low relative pressures) and mesopores (as indicated by the adsorption of N_2 at high relative pressures). Nevertheless, the porosity of the SiO_2@CSs is always lower than that of the corresponding hollow CSs, and the specific surface area (S_{BET}) of the SiO_2@CSs ranged from 115 to 144 $m^2\ g^{-1}$, while the S_{BET} of the CSs ranged from 271 to 602 $m^2\ g^{-1}$. This trend becomes more obvious when the textural properties given in Table 2 are compared, and it can be explained by the higher content of less porous silica

(S_{BET} ≈ 20 m^2 g^{-1}, as determined elsewhere [28]) in the SiO_2@CSs (as discussed in SEM-EDS analysis and TGA).

A closer look of the results obtained for CSs with an E/W volumetric ratio of 2 allows further highlighting the effect of silica etching on the textural properties of the materials. As determined by TGA, the estimated carbon content of SiO_2@CS_2 is 19 wt.%, which is 5.1-fold lower than that of CS_2 (97 wt.%, as given in Table 1). At the same time, the S_{BET} of SiO_2@CS_2 (115 m^2 g^{-1}) is 4.7-fold lower than that of CS_2 (545 m^2 g^{-1}, as given in Table 2), and the mesoporous surface area (S_{Meso}) is 4.9-fold lower. These observations suggest that the textural properties of the carbon phase are negligibly affected by the etching process with NaOH, as the increase of the surface area can be explained by the removal of silica. Regarding the pore volume, two different trends can be observed. On the one hand, the micropore volume (V_{Micro}; corresponding to pores < 2 nm) increases 4.6-fold upon removing the silica core (from 0.023 cm^3 g^{-1} in SiO_2@CS_2, to 0.105 cm^3 g^{-1} in CS_2, as given in Table 2), which can be explained as discussed above for the surface area. On the other hand, the total pore volume (V_{Total}) of CS_2 (1.912 cm^3 g^{-1}) is 6.3-fold higher than that of SiO_2@CS_2 (0.305 cm^3 g^{-1}, as given in Table 2), suggesting a contribution of the hollow core towards the porosity (pores > 2 nm) of CS_2. Similar trends are observed for the CSs prepared with E/W volumetric ratios of 4.5 and 7. Briefly, the S_{BET} of $CS_{4.5}$ (271 m^2 g^{-1}) is 2-fold higher than that of SiO_2@$CS_{4.5}$ (137 m^2 g^{-1}), while the estimated carbon content of $CS_{4.5}$ is 2.3-fold higher than that of SiO_2@$CS_{4.5}$; and the S_{BET} of CS_7 (602 m^2 g^{-1}) is 4.2-fold higher than that of SiO_2@CS_7 (144 m^2 g^{-1}), while the estimated carbon content of CS_7 is 3.5-fold higher than that of SiO_2@CS_7. Moreover, a contribution of the hollow cores towards porosity is also suggested in these cases, as the V_{Total} of the materials prepared with E/W volumetric ratios of 4.5 and 7 increase 6 and 10.8-fold upon etching the silica cores, respectively.

Table 2. Specific surface area (S_{BET}), non-microporous surface area (S_{Meso}), micropore volume (V_{Micro}) and total pore volume (V_{Total}) of the CSs.

Sample	S_{BET} / m^2 g^{-1}	S_{Meso} / m^2 g^{-1}	V_{Micro} / cm^3 g^{-1}	V_{Total} / cm^3 g^{-1}
SiO_2@CS_2	115	59	0.023	0.305
CS_2	545	288	0.105	1.912
SiO_2@$CS_{4.5}$	137	57	0.033	0.159
$CS_{4.5}$	271	122	0.065	0.960
SiO_2@CS_7	144	43	0.042	0.143
CS_7	602	392	0.083	1.548

The results obtained in the pH drift tests performed to determine the pH_{PZC} (Table S2) demonstrate that all the CSs possess a basic nature ($pH_{PZC} \geq 7.9$), although this character is more pronounced in the case of $CS_{4.5}$ and CS_7 ($pH_{PZC} \approx 10$).

3.3. Kinetic adsorption experiments

Kinetic adsorption experiments were conducted with two main objectives, namely to (i) determine the time needed to reach the adsorption equilibrium (to be used in the adsorption equilibrium experiments discussed in Section 3.4), and (ii) study the effect of the hollow core of the CSs on the adsorption performance. The material prepared with the E/W volumetric ratio of 2 was selected for the kinetic study herein reported.

Two preliminary experiments were carried out with SiO_2@CS_2 and CS_2 for 96 h (data not shown). In the case of SiO_2@CS_2, the adsorption capacity for both DCF and VFX was negligible during the whole assays. On the other hand, the time needed for the adsorption equilibrium to be reached in the case of CS_2 was below 24 h regardless of the OMP considered. Thus, the subsequent experiments were performed for 24 h, including experiments performed

in triplicate with CS_2 (Fig. 5). As observed, the adsorption capacity at a given time (q_t) reached a plateau at around 4 to 6 h, both in the case of DCF and VFX, confirming that the adsorption equilibrium was reached under these conditions. Moreover, kinetic modelling was performed (details in Text S1 and Table S3) and all the models could reasonably fit to the experimental data. Among the models studied, namely fractional power, pseudo-first order, pseudo-second order, and Elovich models (Eqs. S1-S4), the pseudo-first order model was found to be the most suitable for fitting the experimental DCF kinetic data and the fractional power model to VFX adsorption data (Fig. 5).

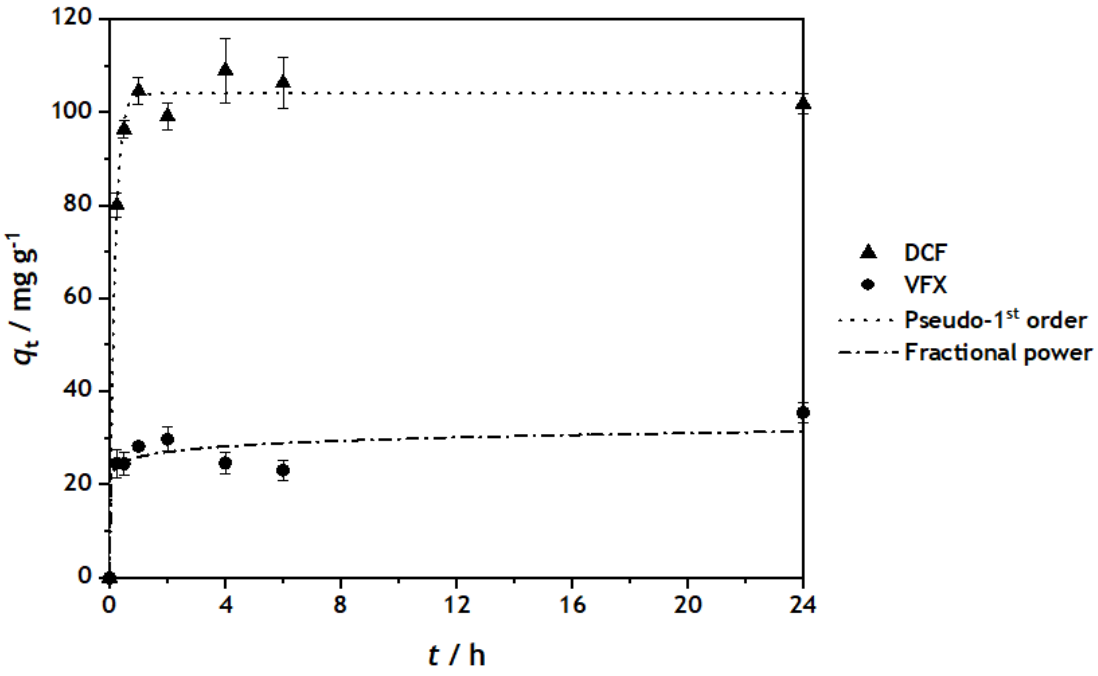

Fig. 5. Kinetic experimental and theoretical data for the adsorption of DCF and VFX onto CS_2. Experiments performed with $[CS_2]$ = 0.25 g L^{-1}, $[DCF]_0$ or $[VFX]_0$ = 100 mg L^{-1}, pH = 6.4 or 6.2 (inherent pH of DCF and VFX solutions, respectively), T = 23 ± 1 ºC (room temperature), and stirring speed of 200 rpm; n = 3.

It was also observed that the adsorption capacity of CS_2 towards DCF is much superior to that of VFX (Fig. 5). This selective affinity can be explained by the different electrostatic interactions established. Considering the solution pH, the p*K*a of the OMPs, and the pH_{PZC} of the adsorbate (Table S4), it can be concluded that the surface of CS_2 is positively charged (pH_{PZC} of CS_2 is 7.9) at the pH of both solutions of DCF and VFX ($pH < pH_{PZC}$ in both cases, as shown in Table S4). Moreover, the pH of the solution containing DCF (6.4) is higher than the p*K*a of this OMP (4.15), revealing that the DCF in solution is (partially) negatively charged. Therefore, electrostatic attraction is expected to occur between the negatively charged DCF and the positively charged surface of CS_2, which explains the higher adsorption performance of this material towards DCF. Contrarily, the pH of the solution containing VFX (6.2) is lower than the p*K*a of this OMP (10.09), revealing that the VFX in solution is (partially) positively charged. Consequently, some electrostatic repulsion is expected to occur between the positively charged VFX and the positively charged surface of CS_2, which explains the lower adsorption performance of this material towards VFX.

In order to understand whether the higher adsorption capacity revealed by CS_2 (when compared to $SiO_2@CS_2$) was due to the higher carbon content of CS_2 or to the presence of the hollow core, additional experiments were designed considering the carbon content obtained from TGA results (Table 1). Accordingly, the adsorbent concentration was normalized by the carbon content, as described in Eq. 1, where $C_{ads,C}$ (g L^{-1}) is the concentration of carbon, C_{ads} is the total adsorbent concentration, and *CC* is the carbon content obtained from TGA (Table 1).

$$C_{ads,C} = C_{ads} \cdot \frac{CC}{100} \quad (1)$$

The $C_{ads,C}$ obtained for CS_2 was 0.2425 g L^{-1}, which is 5.1-fold higher than that of $SiO_2@CS_2$ (0.0475 g L^{-1}). Therefore, an additional experiment was performed with a higher concentration of $SiO_2@CS_2$ (1.28 g L^{-1}; Fig. 6), corresponding to the same $C_{ads,C}$ as that in the experiment

performed with CS_2 (Fig. 5). Comparing the results shown in Fig. 5 with those in Fig. 6, it is observed that CS_2 (Fig. 5) still performs better than $SiO_2@CS_2$ (Fig. 6). Specifically, the maximum q_t obtained for DCF and VFX onto CS_2 was 102 and 36 mg g^{-1}, respectively, whereas onto $SiO_2@CS_2$ (determined on the same basis, *i.e.*, considering the carbon content only) it was 85 and 23 mg g^{-1}, respectively. Bearing this in mind, it can be concluded that the hollow core of CS_2 is, in fact, beneficial for the adsorption of both DCF and VFX, suggesting that these hollow carbon structures can be used as nanocontainers for OMPs.

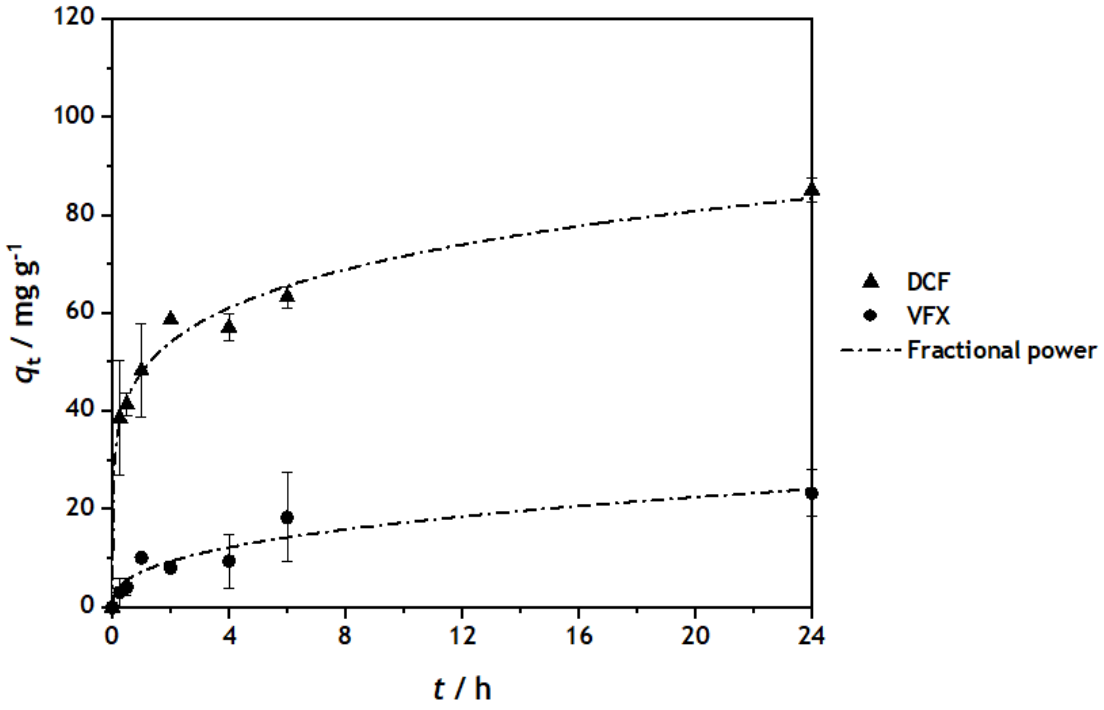

Fig. 6. Kinetic experimental and theoretical data for the adsorption of DCF and VFX onto $SiO_2@CS_2$. Experiments performed with [$SiO_2@CS_2$] = 1.28 g L^{-1} (corresponding to $C_{ads,C}$ = 0.2425 g L^{-1}), $[DCF]_0$ or $[VFX]_0$ = 100 mg L^{-1}, pH = 6.4 or 6.2 (inherent pH of DCF and VFX solutions, respectively), T = 23 ± 1 ºC (room temperature), and stirring speed of 200 rpm; n = 2. q_t values obtained considering the $C_{ads,C}$ only. Detailled kinetic modeling data is given in Table S5.

3.4. Equilibrium adsorption experiments

Equilibrium adsorption experiments were then conducted with two main objectives, namely to (i) evaluate the adsorption capacity of the hollow CSs, and (ii) study the effect of particle size on the adsorption performance. In this case the non-linearized forms of the Langmuir, Freundlich, and Sips models (Eqs. S5-S7) were studied (Text S2 and Table 3). As somehow expected, the Sips model (3-parameter isotherm model) was found to be the most suitable for fitting the experimental data (Fig. 7).

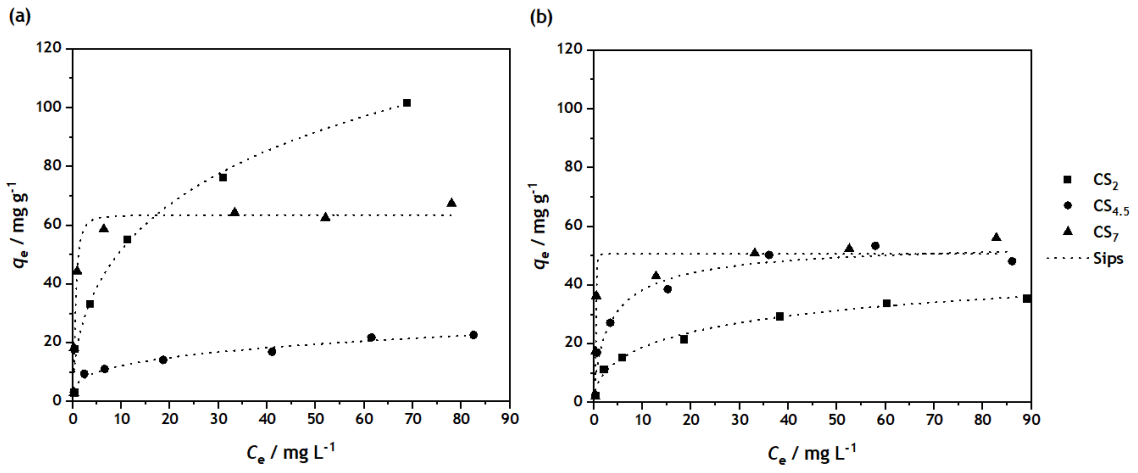

Fig. 7. Experimental and theoretical data for the adsorption isotherms of (a) DCF and (b) VFX onto CS_2, $CS_{4.5}$ or CS_7. Experiments performed with $[CS_X]$ = 0.25 g L^{-1}, $[DCF]_0$ or $[VFX]_0$ = 1, 5, 10, 25, 50, 75, and 100 mg L^{-1}, T = 23 ± 1 ºC (room temperature), t = 24 h, and stirring speed of 200 rpm.

Overall, the adsorption capacity of the hollow CSs towards DCF is higher than the adsorption capacity towards VFX. As discussed in Section 3.3, this can be explained by the different electrostatic interactions established in each case (*i.e.*, some electrostatic attraction between the

surface of the CSs and DCF, and some electrostatic repulsion between the surface of the CSs and VFX). Specifically, CS_2 and CS_7 revealed better adsorption capacity for DCF than $CS_{4.5}$ (Fig. 7a), which may be explained by enhanced surface area and porosity of CS_2 and CS_7 when compared to $CS_{4.5}$ (Table 3). In the case of VFX (Fig. 7b), $CS_{4.5}$ and CS_7 showed similar adsorption capacities, which were both higher than the adsorption capacity revealed by CS_2. These results cannot be explained only by the different textural properties of the materials, nor by the electrostatic interactions previously discussed. Nevertheless, the higher pH_{PZC} of $CS_{4.5}$ and CS_7 ($\approx$ 10) compared to that of CS_2 (7.9), suggests that other adsorption mechanisms, such as chemisorption, may also be involved. The better adsorption performance over the concentration range under study was obtained with CS_7, regardless of the OMP considered. However, despite this better adsorption performance obtained with the hollow CSs with larger particle size (*i.e.*, CS_7, with $d_{average}$ of (284 ± 32) nm), no evident correlations were obtained between the adsorption performance and the particle size of the hollow CSs. Nevertheless, the effectiveness of silica dissolution was not similar for the different materials.

Table 3. Equilibrium model parameters (non-linearized form equations) for the adsorption of DCF and VFX onto the hollow CSs.

	Langmuir			Freundlich			Sips			
	q_{sat} / mg g^{-1}	K_L / L mg^{-1}	r^2	K_F / L mg^{-1}	n_F	r^2	q_m / mg g^{-1}	K_s / L mg^{-1}	n_S	r^2
DCF										
CS_2	109.66	0.10	0.9542	20.87	2.65	0.9840	259.80	0.01	2.04	0.9871
$CS_{4.5}$	21.81	0.19	0.8812	6.33	3.46	0.9769	56.84	3.77×10^{-3}	2.83	0.9769
CS_7	66.36	1.31	0.9312	31.03	5.15	0.7646	63.60	1.72	0.54	0.9608
VFX										
CS_2	37.05	0.12	0.9569	8.23	2.96	0.9792	61.45	0.02	1.87	0.9888
$CS_{4.5}$	51.69	0.37	0.9498	17.55	3.83	0.8914	56.02	0.27	1.30	0.9576
CS_7	52.32	1.39	0.8047	23.70	4.87	0.7726	50.64	2.21	0.19	0.9143

Regarding equilibrium modeling, the Sips model (3-parameter isotherm model) showed the highest values of r^2 (Table 3), suggesting that adsorption is taking place on both homogeneous and heterogeneous surface of the CSs. Among the 2-parameter isotherm models (*i.e.*, Freundlich and Langmuir), the Langmuir model was the best to predict the adsorption of both OMPs onto CS_7, and the Freundlich model was the most suitable to predict adsorption on CS_2. $CS_{4.5}$ revealed different behavior depending on the OMP considered; in this case, the adsorption of DCF and VFX was better described by the Freundlich and Langmuir models, respectively.

A literature review on the application of carbon-based materials for adsorption of DCF (Table 4) and VFX (Table 5) was performed to compare the performance of the previously reported materials with those of the CSs for removing DCF and VFX. Overall, the performances obtained with the CSs developed in this study are above the average of those previously reported, thus highlighting the potential of these hollow carbon nanocontainers as efficient

adsorbents for DCF removal (Table 4). It is important to note that the higher capacities reported in the literature may be due, essentially, to the higher surface area of the material, the change of the solution pH, and/or the change of the adsorbent concentration. The developed CSs, on the other hand, perform better compared to the materials tested in the only work found in the literature on the adsorption of VFX (Table 5).

Table 4. Comparison of the performance of several reported carbon-based materials developed as adsorbents of DCF[a].

Reference	Adsorbent	Adsorption conditions	S_{BET} / $m^2\ g^{-1}$	Maximum capacity / mg g^{-1}	Isotherm
This study	**CS_2**	Ultrapure water, $pH_{solution}$ = 6.4, C_{ads} = 0.25 g L^{-1}, C_0 = 1 – 100 mg L^{-1}, T = 23 ºC, t = 24 h	545	259.80	Sips
	$CS_{4.5}$		271	56.84	Sips
	CS_7		602	63.60	Sips
Rigueto *et al.*, 2021 [29]	**Commercial gelatin powder with carbon nanotubes**	n/d, $pH_{solution}$ = 8.15, C_{ads} = 2.0 g L^{-1}, C_0 = 37.5 – 300 mg L^{-1}, T = 25 ºC, t = 2.5 h	133	26.97	Freundlich
Kimbi Yaah *et al.*, 2021 [30]	**Hydrochar-derived adsorbent**	Deionized water, $pH_{solution}$ = 2.0, C_{ads} = 15 g L^{-1}, C_0 = 0 – 50 mg L^{-1}, T = 25 ºC, t = 1.5 h	131	13.16	Langmuir
Salvestrini *et al.*, 2020 [31]	**Commercial activated carbon, Filtrasorb 400**	Pure water, $pH_{solution}$ = 6.8, C_{ads} = 0.5 g L^{-1}, C_0 = 24 - 218 mg L^{-1}, T = n/d, t = 120 h	1000	180	Langmuir
Khalil *et al.*, 2020 [32]	**Graphene**	n/d, $pH_{solution}$ = 7.5, C_{ads} = 0.25 g L^{-1}, C_0 = 0.1 - 100 mg L^{-1}, T = 22, t = 24 h	670	76	Sips
Álvarez-Torrellas *et al.*, 2018 [33]	**Carbide-derived carbons produced at 1000ºC**	Deionized water, $pH_{solution}$ = n/d, C_{ads} = 0.3 g L^{-1}, C_0 = 10 – 100 mg L^{-1}, T = 30 ºC, t = 1 h	1676	523	n/d
Jauris, *et al.*, 2016 [34]	**Reduced graphene oxide**	Deionized water, $pH_{solution}$ = 10.0, C_{ads} = 1.5 g L^{-1}, C_0 = 20 - 200 mg L^{-1}, T = 25 ºC, t = 3.3 h	98	59.67	Liu [b]

Bhadra *et al.*, 2016 [35]	**Activated carbons oxidized with ammonium persulfate**	Water, $pH_{solution}$ = 5.5, C_{ads} = 0.2 g L^{-1}, C_0 = 25 – 100 mg L^{-1}, T = 25 ºC, t = 24 h	704	487	Langmuir
Bernardo *et al.*, 2016 [36]	**Potato peel waste-based activated carbon**	Deionized water, $pH_{solution}$ = 5, C_{ads} = 0.4 g L^{-1}, C_0 = 10 - 100 mg L^{-1}, T = 25 ºC, t = 17 h	866	68.5	Langmuir

[a] Data collected from Scopus on June 24, 2021, using the following query: "carbon AND adsorption AND diclofenac AND Chemical Engineering AND Environmental Science".

[b] the authors used *Liu* as an isotherm model.

n/d no data.

Table 5. Comparison of the performance of several reported carbon-based materials developed as adsorbents of VFX[a].

Reference	Adsorbent	Adsorption conditions	S_{BET} / $m^2\ g^{-1}$	Maximum capacity / mg g^{-1}	Isotherm
This study	**CS_2**	Ultrapure water, $pH_{solution}$ = 6.2, C_{ads} = 0.25 g L^{-1}, C_0 = 1 – 100 mg L^{-1}, T = 23 ºC, t = 24 h	545	61.45	Sips
	$CS_{4.5}$		271	56.02	Sips
	CS_7		602	50.64	Sips
Calisto *et al.*, 2015 [37]	**Commercial activated carbon**	Ultrapure water, $pH_{solution}$ = 7.0, C_{ads} = 0.02 – 0.12 g L^{-1}, C_0 = 5 mg L^{-1}, T = 25 ºC, t = 0.5 h	848	42.5	Langmuir
	Non-activated carbon produced by pyrolysis of paper mill sludge	Ultrapure water, $pH_{solution}$ = 10.5, C_{ads} = 0.15 – 4.0 g L^{-1}, C_0 = 5 mg L^{-1}, T = 25 ºC, t = 0.5 h	209	8.5	Langmuir

[a] Data collected from Scopus on June 24, 2021, using the following query: "carbon AND adsorption AND venlafaxine AND Chemical Engineering AND Environmental Science".

n/d no data.

4. Conclusions

The carbon-based materials with three different sizes that were developed for the removal of DCF and VFX from aqueous solution have a spherical morphology, the particle size increasing with the E/W volumetric ratio. The S_{BET}, microporous and mesoporous structure of the CSs were more pronounced than in the SiO_2@CSs, which means that the silica core influenced the porosity of the materials. The pH_{PZC} of the CSs ranged from 7.9 to 10.1, revealing their basic character. The positive impact of the hollow core was demonstrated, with the adsorption process reaching the equilibrium in less than 24 h. Moreover, it was proved that the higher adsorption capacity of CS_2 was mainly related to the hollow core and not to the superior carbon fraction that this material possesses when compared to SiO_2@CS_2 (*i.e.*, prior to silica dissolution). Equilibrium studies demonstrated that CS_7 was the material presenting the best compromise for the adsorption of both OMPs. Moreover, this carbon material shows the best removals at lower concentrations of adsorbate. Therefore, the synthesized materials are promising for the removal of DCF and VFX from water.

Acknowledgments

This work was financially supported by: Project PTDC/QUI-QAN/30521/2017 - POCI-01-0145-FEDER-030521 - funded by FEDER funds through COMPETE2020 - Programa Operacional Competitividade e Internacionalização (POCI) and by national funds (PIDDAC) through FCT/MCTES. We would also like to thank the scientific collaboration under Base Funding - UIDP/50020/2020 of the Associate Laboratory LSRE-LCM - funded by national funds through FCT/MCTES (PIDDAC). ARLR acknowledges FCT funding under DL57/2016 Transitory Norm Programme. Technical assistance with SEM analysis is gratefully acknowledged to CEMUP team.

References

[1] T. Deblonde, C. Cossu-Leguille, P. Hartemann, Emerging pollutants in wastewater: A review of the literature, Int. J. Hyg. Environ. Health. 214 (2011) 442–448. https://doi.org/10.1016/j.ijheh.2011.08.002.

[2] A.M. Gorito, A.R. Ribeiro, C.M.R. Almeida, A.M.T. Silva, A review on the application of constructed wetlands for the removal of priority substances and contaminants of emerging concern listed in recently launched EU legislation, Environ. Pollut. 227 (2017) 428–443. https://doi.org/10.1016/j.envpol.2017.04.060.

[3] T.K. Sen, Physical Chemical and Biological Treatment Processes for Water and Wastewater, (2014) 1–28. http://search.ebscohost.com/login.aspx?direct=true&AuthType=ip,uid&db=e230xww&AN=1084472&lang=pt-pt&site=ehost-live&scope=site (accessed April 17, 2021).

[4] E. Commission, River basin management - Water - Environment, (n.d.). https://ec.europa.eu/environment/water/water-framework/index_en.html (accessed February 23, 2021).

[5] A. Rubirola, J. Quintana, M.R. Boleda, M.T. Galceran, Analysis of 32 priority substances from EU water framework directive in wastewaters, surface and drinking waters with a fast sample treatment methodology, Int. J. Environ. Anal. Chem. 99 (2019) 16–32. https://doi.org/10.1080/03067319.2019.1571195.

[6] S. Lacorte, S. Luis, C. Gómez-Canela, T. Sala-Comorera, A. Courtier, B. Roig, A.M. Oliveira-Brett, C. Joannis-Cassan, J.I. Aragonés, L. Poggio, T. Noguer, L. Lima, C. Barata, C. Calas-Blanchard, Pharmaceuticals released from senior residences: occurrence and risk evaluation, Environ. Sci. Pollut. Res. 25 (2018)

6095–6106. https://doi.org/10.1007/s11356-017-9755-1.

[7] J. Hartmann, P. Bartels, U. Mau, M. Witter, W. v. Tümpling, J. Hofmann, E. Nietzschmann, Degradation of the drug diclofenac in water by sonolysis in presence of catalysts, Chemosphere. 70 (2008) 453–461. https://doi.org/10.1016/j.chemosphere.2007.06.063.

[8] C.D. Metcalfe, S. Chu, C. Judt, H. Li, K.D. Oakes, M.R. Servos, D.M. Andrews, Antidepressants and their metabolites in municipal wastewater, and downstream exposure in an urban watershed, Environ. Toxicol. Chem. 29 (2010) 79–89. https://doi.org/10.1002/ETC.27.

[9] M.J. Arlos, L.M. Bragg, M.R. Servos, W.J. Parker, Simulation of the fate of selected pharmaceuticals and personal care products in a highly impacted reach of a Canadian watershed, Sci. Total Environ. 485–486 (2014) 193–204. https://doi.org/10.1016/j.scitotenv.2014.03.092.

[10] V. Koutsouba, T. Heberer, B. Fuhrmann, K. Schmidt-Baumler, D. Tsipi, A. Hiskia, Determination of polar pharmaceuticals in sewage water of Greece by gas chromatography-mass spectrometry, Chemosphere. 51 (2003) 69–75. https://doi.org/10.1016/S0045-6535(02)00819-6.

[11] M. Tripathy, S. Padhiari, G. Hota, L-Cysteine-Functionalized Mesoporous Magnetite Nanospheres: Synthesis and Adsorptive Application toward Arsenic Remediation, J. Chem. Eng. Data. 65 (2020) 3906–3919. https://doi.org/10.1021/acs.jced.0c00250.

[12] M. Khajeh, S. Laurent, K. Dastafkan, Nanoadsorbents: Classification, preparation, and applications (with emphasis on aqueous media), Chem. Rev. 113 (2013) 7728–7768. https://doi.org/10.1021/cr400086v.

[13] A.B. Fuertes, P. Valle-Vigón, M. Sevilla, One-step synthesis of silica@resorcinol-

formaldehyde spheres and their application for the fabrication of polymer and carbon capsules, Chem. Commun. 48 (2012) 6124–6126. https://doi.org/10.1039/c2cc32552g.

[14] D.L.D. Lima, C.P. Silva, M. Otero, Dispersive liquid-liquid microextraction for the quantification of venlafaxine in environmental waters, J. Environ. Manage. 217 (2018) 71–77. https://doi.org/10.1016/j.jenvman.2018.03.060.

[15] M. Llorca, F. Castellet-Rovira, M.J. Farré, A. Jaén-Gil, M. Martínez-Alonso, S. Rodríguez-Mozaz, M. Sarrà, D. Barceló, Fungal biodegradation of the N-nitrosodimethylamine precursors venlafaxine and O-desmethylvenlafaxine in water, Environ. Pollut. 246 (2019) 346–356. https://doi.org/10.1016/j.envpol.2018.12.008.

[16] Y. Zhang, S.U. Geißen, C. Gal, Carbamazepine and diclofenac: Removal in wastewater treatment plants and occurrence in water bodies, Chemosphere. 73 (2008) 1151–1161. https://doi.org/10.1016/j.chemosphere.2008.07.086.

[17] E. Commission, Commission Implementing Decision (EU) 2015/ 495, 2015. https://eur-lex.europa.eu/legal-content/EN/TXT/PDF/?uri=CELEX:32015D0495&from=EN (accessed March 10, 2021).

[18] E. Commission, Commission Implementing Decision (EU) 2020/1161, 2020. https://eur-lex.europa.eu/legal-content/EN/TXT/PDF/?uri=CELEX:32020D1161&from=EN (accessed March 12, 2021).

[19] J. Wang, X. Guo, Adsorption isotherm models: Classification, physical meaning, application and solving method, Chemosphere. 258 (2020) 127279. https://doi.org/10.1016/j.chemosphere.2020.127279.

[20] M. Thommes, K. Kaneko, A. V. Neimark, J.P. Olivier, F. Rodriguez-Reinoso, J. Rouquerol, K.S.W. Sing, Physisorption of gases, with special reference to the evaluation of surface area and pore size distribution (IUPAC Technical Report), Pure Appl. Chem. 87 (2015) 1051–1069. https://doi.org/10.1515/pac-2014-1117.

[21] R.S. Ribeiro, Z. Frontistis, D. Mantzavinos, D. Venieri, M. Antonopoulou, I. Konstantinou, A.M.T. Silva, J.L. Faria, H.T. Gomes, Magnetic carbon xerogels for the catalytic wet peroxide oxidation of sulfamethoxazole in environmentally relevant water matrices, Appl. Catal. B Environ. 199 (2016) 170–186. https://doi.org/10.1016/j.apcatb.2016.06.021.

[22] W. Stöber, A. Fink, E. Bohn, Controlled growth of monodisperse silica spheres in the micron size range, J. Colloid Interface Sci. 26 (1968) 62–69. https://doi.org/10.1016/0021-9797(68)90272-5.

[23] M.T. Harris, R.R. Brunson, C.H. Byers, The base-catalyzed hydrolysis and condensation reactions of dilute and concentrated TEOS solutions, J. Non. Cryst. Solids. 121 (1990) 397–403. https://doi.org/10.1016/0022-3093(90)90165-I.

[24] G.H. Bogush, C.F. Zukoski IV, Studies of the kinetics of the precipitation of uniform silica particles through the hydrolysis and condensation of silicon alkoxides, J. Colloid Interface Sci. 142 (1991) 1–18. https://doi.org/10.1016/0021-9797(91)90029-8.

[25] A. Van Blaaderen, J. Van Geest, A. Vrij, Monodisperse colloidal silica spheres from tetraalkoxysilanes: Particle formation and growth mechanism, J. Colloid Interface Sci. 154 (1992) 481–501. https://doi.org/10.1016/0021-9797(92)90163-G.

[26] K.S. Rao, K. El-Hami, T. Kodaki, K. Matsushige, K. Makino, A novel method for synthesis of silica nanoparticles, J. Colloid Interface Sci. 289 (2005) 125–131.

https://doi.org/10.1016/j.jcis.2005.02.019.

[27] A.H. Lu, G.P. Hao, Q. Sun, Can carbon spheres be created through the stöber method?, Angew. Chemie - Int. Ed. 50 (2011) 9023–9025. https://doi.org/10.1002/anie.201103514.

[28] M. Szekeres, J. Tóth, I. Dékány, Specific surface area of stoeber silica determined by various experimental methods, Langmuir. 18 (2002) 2678–2685. https://doi.org/10.1021/la011370j.

[29] C.V.T. Rigueto, M. Rosseto, M.T. Nazari, B.E.P. Ostwald, I. Alessandretti, C. Manera, J.S. Piccin, A. Dettmer, Adsorption of diclofenac sodium by composite beads prepared from tannery wastes-derived gelatin and carbon nanotubes, J. Environ. Chem. Eng. 9 (2021) 105030. https://doi.org/10.1016/j.jece.2021.105030.

[30] V.B. Kimbi Yaah, M. Zbair, S. Botelho de Oliveira, S. Ojala, Hydrochar-derived adsorbent for the removal of diclofenac from aqueous solution, Nanotechnol. Environ. Eng. 6 (2021) 3. https://doi.org/10.1007/s41204-020-00099-5.

[31] S. Salvestrini, A. Fenti, S. Chianese, P. Iovino, D. Musmarra, Diclofenac sorption from synthetic water: Kinetic and thermodynamic analysis, J. Environ. Chem. Eng. 8 (2020) 104105. https://doi.org/10.1016/j.jece.2020.104105.

[32] A.M.E. Khalil, F.A. Memon, T.A. Tabish, D. Salmon, S. Zhang, D. Butler, Nanostructured porous graphene for efficient removal of emerging contaminants (pharmaceuticals) from water, Chem. Eng. J. 398 (2020) 125440. https://doi.org/10.1016/j.cej.2020.125440.

[33] S. Álvarez-Torrellas, M. Munoz, J. Gläsel, Z.M. de Pedro, C.M. Domínguez, J. García, B.J.M. Etzold, J.A. Casas, Highly efficient removal of pharmaceuticals from water by well-defined carbide-derived carbons, Chem. Eng. J. 347 (2018)

595–606. https://doi.org/10.1016/j.cej.2018.04.127.

[34] I.M. Jauris, C.F. Matos, C. Saucier, E.C. Lima, A.J.G. Zarbin, S.B. Fagan, F.M. Machado, I. Zanella, Adsorption of sodium diclofenac on graphene: A combined experimental and theoretical study, Phys. Chem. Chem. Phys. 18 (2016) 1526–1536. https://doi.org/10.1039/c5cp05940b.

[35] B.N. Bhadra, P.W. Seo, S.H. Jhung, Adsorption of diclofenac sodium from water using oxidized activated carbon, Chem. Eng. J. 301 (2016) 27–34. https://doi.org/10.1016/j.cej.2016.04.143.

[36] M. Bernardo, S. Rodrigues, N. Lapa, I. Matos, F. Lemos, M.K.S. Batista, A.P. Carvalho, I. Fonseca, High efficacy on diclofenac removal by activated carbon produced from potato peel waste, Int. J. Environ. Sci. Technol. 13 (2016) 1989–2000. https://doi.org/10.1007/s13762-016-1030-3.

[37] V. Calisto, C.I.A. Ferreira, J.A.B.P. Oliveira, M. Otero, V.I. Esteves, Adsorptive removal of pharmaceuticals from water by commercial and waste-based carbons, J. Environ. Manage. 152 (2015) 83–90. https://doi.org/10.1016/j.jenvman.2015.01.019.